***Proceedings of the IASS 2024 Symposium***
*Redefining the Art of Structural Design*
August 26-30, 2024, Zurich Switzerland
Philippe Block, Giulia Boller, Catherine DeWolf,
Jacqueline Pauli, Walter Kaufmann (eds.)

# Super-long span aluminum alloy mega-latticed structures

Qingwen ZHANG*, Yilinke TAN[a], Guolong ZHANG, Yu ZHANG, Feng FAN

* School of Civil Engineering, Harbin Institute of Technology
Huanghe Road 73, Harbin 150090, China
zhangqw@hit.edu.cn

[a] School of Architecture and Civil Engineering, Xihua University

## Abstract

The mega-latticed structure is a new type of spatial structure, which has clear priorities and concise force transmission lines and is regarded as a good choice for super-long span spatial structures. However, with increasing spans, structural self-weight has become the key issue restricting further development. This paper first explores the applicable analysis methods for the mega-latticed structure and discusses the effect of joint stiffness on the overall structural performance. To find a suitable material and form for super-long span mega-latticed structures, a comparison of the static properties and stability of the structure is undertaken using ANSYS. It is a Three-dimensional grid type mega-latticed structure using steel and aluminum alloy, with spans from 800m to 1200m. Both geometric and material nonlinearity are taken into consideration in the stability analysis. Based on the arc-length method, load-displacement curves and ultimate loads are obtained. The force distribution in the structures is illustrated and discussed, and the reasons for the differences between these structures are examined. It is found that both structures had good mechanical performance, but the aluminum alloy structures have much better economic indices for spans greater than 1000m. The material consumption of the aluminum alloy structures is 1/3-1/7 of those of the steel structures with spans from 800m to 1200m, indicating that the aluminum alloy structures have better economic performance at larger spans. In addition, aluminum alloy structures are more sensitive to wind but less sensitive to node imperfections and elastoplastic stability. This work provides a reference for the design and application of aluminum alloy mega-latticed structures.

**Keywords**: mega-latticed structure, city dome, super-long span, aluminum alloy, static properties, stability, load-displacement curves, semi-rigid connection.

## 1. Introduction

## 1. Introduction

In recent decades, there has been an increasing demand for a longer span of spatial structure, as mentioned in Makowski [1] and EI-Sheikh [2]. With the development of society and climate change, some attention has been drawn to the feasibility of super-long span spatial structures, considering various requirements, such as residential area establishment under bad environments, city protection against extreme climate, energy conservation, and emission reduction. Some plans have been discussed, such as the famous Manhattan Dome and the City of North Pole proposed by Fuller and Otto, respectively. However, these plans are still under discussion because of material and technical limitations. Therefore, it is needed to research some more feasible and practical structure forms and materials for super-long-span spatial structures.

Recently, a novel mega-latticed structure, with clear priorities and concise force transmission lines, are regarded as a good choice for super-long span spatial structures. This structure, which consists of a main

structure and its substructures, has been promoted by He et al. [3]. The stability of cylindrical reticulated mega-structures, with various substructures in He et al. [4-6], have been studied and a series of key parameters were analyzed in detail. The formation and stability in the construction of a Ribbed type reticulated mega-structure in He et al. [7] were first investigated. Subsequently, a Kiewitt-type mega-latticed structure in Zhang et al. [8], a Geodesic and a Three-dimensional grid-type mega-latticed structure in Zhang and Tan et al. [9, 10], and a morphology-optimized surface structure in Tan et al. [11] were proposed and have been shown to have good applicability for spans of 800m to 1200m. The above structures were all researched with steel material. However, with increasing spans, steel consumption has become the key issue that restricts further development. Aluminum alloy, with a higher strength-weight ratio and good corrosion resistance, has been applied in more and more spatial structures. These aluminum alloy structures have drawn the attention of some researchers. Mazzolani [12] studied the design and application of 3D aluminum structures by referring to real cases. Xiong et al. [13, 14] conducted experimental and numerical studies on single-layer reticulated shells with aluminum alloy gusset joints. These researches have shown the good performance of aluminum alloy and advised on the application of aluminum alloy structures, suggesting that this material might be suitable for super-long span spatial structures.

In this paper, an aluminum alloy mega-latticed structure was automatically generated using ANSYS Parameter Design Language (APDL). These structures were: Three-dimensional grid-type mega-latticed structures. Subsequently, the joint stiffness of the structures was discussed and a proper simulation method for the joints in the FE model was proposed. Based on mechanical performance and economic indices, analysis of these two structures with spans from 800m to 1200m has been carried out, by emphasizing the peculiar differences with steel ones. The reasons for these differences were analyzed in detail. This work shows that aluminum alloy is a reasonable material for super-long-span mega-latticed structures.

## Structural configuration and analytical method

### 2.1. Structural configuration

This paper focuses on the main structure of super-long span mega-latticed structures. It has been shown that the Three-dimensional grid-type mega-latticed structures have excellent mechanical performance and a good economic index for steel with spans of 800m, 1000m, and 1200m, as mentioned in Zhang et al. [9]. In this paper, the use of steel and aluminum alloy is examined for constructing Three-dimensional grid type structures, similar to those shown in Figure 1.

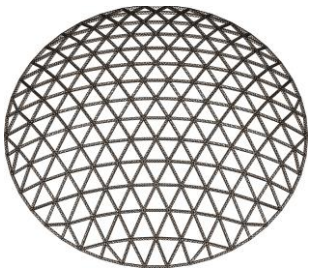

Figure 1: Three-dimensional grid-type mega-latticed structures.

The geometric parameters of these two structures are shown in Figure 2. This includes the span $L$, the rise $H$, and the 3D trussed beams with internode length $m$, height $h$, and width $b$. In addition, the circumferential divisions $C_g$, $C_t$ ($C_g$ and $C_t$ represent the circumferential divisions of the Three-dimensional structures, respectively) and the number of radial grids $R$ were considered as key parameters, which decides the length of the 3D trussed beams and the angle between them. Triangular sections have been suggested as being reasonable for the 3D trussed beams and provide good stability by Zhang et al. [8]. The 3D trussed beams were triangular and connected using pyramid joints (as illustrated in Figure 2(b)). The structures were supported by fixed-hinged supports at the main nodes of the surrounding

bottom chords. Round tubes were used for various members. The material properties of steel and aluminum alloy adopted in this paper are shown in Table 1.

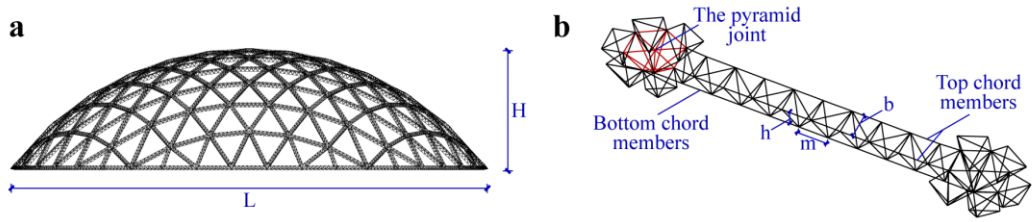


Figure 2: Geometric parameters and topological forms of the structure, a) macro parameters of the Three-dimensional grid type structures, b) parameters and form of the 3D trussed beams.

Table 1: Material properties of steel and aluminum alloy.

| Material properties | Steel (Q420) | Aluminum alloy (6061-T6) |
|---|---|---|
| Yield strength (MPa) | 420 | 240 |
| Elastic modulus (GPa) | 210 | 70 |
| Density (kg/m$^3$) | 7850 | 2700 |
| Poisson's ratio | 0.3 | 0.3 |
| Thermal expansion coefficient (/°C) | $1.2\times10^{-5}$ | $2.4\times10^{-5}$ |

## 2.2. Analytical method

For static analysis, the loads considered in this paper are as follows. Because of the different densities of steel and aluminum alloy, uniform dead loads (including self-weight of substructures and hangings) of 1.4kN/m$^2$ and 0.7kN/m$^2$ were applied to the steel and aluminum alloy structures, respectively. The whole-span or half-span uniform live load was 0.5kN/m$^2$. The joint self-weight was considered by multiplying each material density by 1.2. The basic wind pressure was 0.7kN/m$^2$ (as suggested in *GB50009-2012, Load Code for the Design of Building Structures* [15]). The above loads were transformed into concentrated forces and applied to the top chord nodes of the 3D trussed beams. Temperature changes of 30°C and -30°C were also considered. Based on the above assumptions, nine load cases were selected, and these are shown in Table 2. It should be noted that load case 9 was special. As stated in the load specification, a revolving shell encounters whole-span wind suction when the shell is subject to a uniform cross wind and the rise-span ratio is less than or equal to 1/4. In addition, an increase in temperature can lead to an upward displacement of the shell. Thus, load case 9 represents the worst situation for upward displacement, especially for aluminum alloy structures due to their lower self-weight and higher thermal expansion coefficient (as mentioned in Section 2.1).

Table 2: Load combination for static analysis.

| Number | Load case | Partial coefficient × combination coefficient | | | |
|---|---|---|---|---|---|
| | | Dead | Live | Wind | Increase (decrease) temperature |
| 1 | Dead + live | 1.35 | 1.4×0.7 | - | - |
| 2 | Dead + live | 1.2 | 1.4×1.0 | - | - |
| 3 | Dead + half-span live | 1.35 | 1.4×0.7 | - | - |
| 4 | Dead + half-span live | 1.2 | 1.4×1.0 | - | - |
| 5 | Dead + live + decrease-temperature | 1.35 | 1.4×0.7 | - | 1.4×0.6 |
| 6 | Dead + live + decrease-temperature | 1.2 | 1.4×1.0 | - | 1.4×0.6 |
| 7 | Dead + half-span live + decrease-temperature | 1.35 | 1.4×0.7 | - | 1.4×0.6 |
| 8 | Dead + half-span live + decrease-temperature | 1.2 | 1.4×1.0 | - | 1.4×0.6 |
| 9 | Dead + wind + increase-temperature | 1.0 | - | 1.4×0.6 | 1.4×0.6 |

Sections of various members were optimized according to the least favorable load case (the maximum displacement or the stress peak is the biggest one among all these cases) in an initial static analysis. When optimizing the member sections, the stress ratios were limited to no bigger than 0.85. The limits

of the tension slenderness ratio and compress slenderness ratio were 250 and 150 for the steel structures and 300 and 150 for the aluminum structures. To achieve a balance between mechanical performance and economic index, and to avoid local buckling of members, the diameter-thickness ratios of members were kept within 30 and 50. Afterwards, static analysis of the structures was conducted again with the optimized member sections and these member sections were used in the following stability analysis.

For the stability analysis, linear and nonlinear analyses were conducted. With the linear stability analysis, eigenvalue buckling loads were obtained and considered as the limit loads for the nonlinear stability analysis. Geometric nonlinearity and double nonlinearity, i.e. including both geometric and material nonlinearity, were taken into consideration in the nonlinear stability analysis. According to Fan et al. [16], the lowest eigenvalue buckling mode of the linear stability analysis was applied to the ideal structure as an initial geometric imperfection, which leads to the lowest ultimate load of the structure. And 1/300 of the span was taken as the maximum imperfection, as suggested in the *Technical Specification for Space Frame Structure (JGJ7-2010)* [17]. Based on the arc-length method in Crisfield [18] and Riks [19], load-displacement curves and ultimate loads were obtained.

## 3. Finite Element Model and the discussion of joint stiffness

The modeling of mega-latticed structures was conducted using the finite element package ANSYS. Element BEAM 188 was selected to simulate various members of the structures. This element has been widely adopted in Zhang et al. [8, 9], Xiong et al. [13] and Fan [20]. It is a linear, quadratic, or cubic two-node 3D element, and is suitable for analyzing slender to moderately stubby/thick beam structures. The element adopts Timoshenko beam theory, includes shear-deformation effects, and provides options for unrestrained warping and restrained warping of cross-sections [21]. Joints between these elements were acquiescently considered as rigid connections, which was different from some practical structures where the joints should be considered as semi-rigid connections.

It has been shown that the joints of some aluminum alloy shell structures should be considered to be semi-rigid connections in Xiong et al. [13], which may dramatically influence the structural stiffness. Thus, it is necessary to study the influence of joint stiffness on the mega-latticed structures. In this section, a Three-dimensional grid type structure with semi-rigid joints was established. It was modeled with a FE model of a member with semi-rigid joints, as shown in Figure 3. This model has been widely adopted by Xiong et al. [13] and Ma et al. [22] and shown to be reliable. It is composed of a member element and two rigid joint zones, simulated with BEAM188. The member element and a rigid joint zone are connected by three springs in three orientations (two moments and one torque) simulated with COMBIN39. The spring element COMBIN39 is a unidirectional element with a nonlinear generalized force-deflection capability that can simulate in-plane bending stiffness, out-of-plane bending stiffness, and torsional stiffness of a joint. Besides, the translations in the x, y, and z orientations of the nodes at the springs were coupled. As there was no experimental data for such gigantic joints and to save calculation cost, the moment-rotation curves of the joints were simplified to be linear and the joint bending stiffness was assumed to be dimensionless parameters from 0.1 to 100000, to represent relative values. The joint bending stiffness 0.1 is close to that of a hinge joint, whilst 100000 is close to that of a rigid joint. According to Ma et al. [22], the joint torsional stiffness was set at 1/10 of the bending stiffness. In addition, the diameters of the rigid joint zone were assumed to be 1.5 times that of the member.

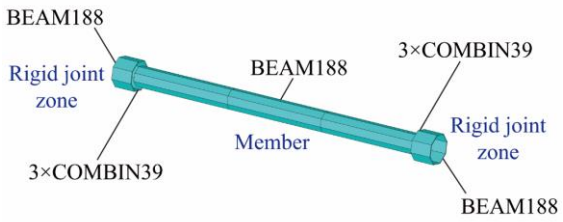


Figure 3: Finite element model of a member with semi-rigid joints.

The static and stability performance of the structures with different joint stiffnesses were calculated and

are shown in Figure 4. The maximum displacements decreased with the increase of the joint stiffness, which means the improvement of structural stiffness. For load case 5, the maximum displacement varied from 1.755 m to 1.813 m, and the relative difference was 3.3%. The ultimate loads also increased with an increase in joint stiffness, and the relative difference was 27.7%. But actually, the joints in an aluminum alloy structure are not complete hinge connections. The relative difference in ultimate loads could be much smaller. Some single-layer elliptical paraboloid latticed shells with semi-rigid joints were studied by Ma et al. [22], and the minimal ratio of the ultimate loads of the shells with semi-rigid joints to those with rigidly jointed shells was 0.24, and this would be smaller for longer spans. The analytical results show that the joint stiffness has a relatively smaller effect on the mega-latticed structures than on single-layer latticed shells. Besides, there are nearly 200 thousand elements in an analytical model with semi-rigid connections, which is four times the quantity of that with rigid connections. Therefore, to save computing time, the joints of the mega-latticed structures in this paper are considered rigid connections, also consider a joint stiffness discount factor of 0.76

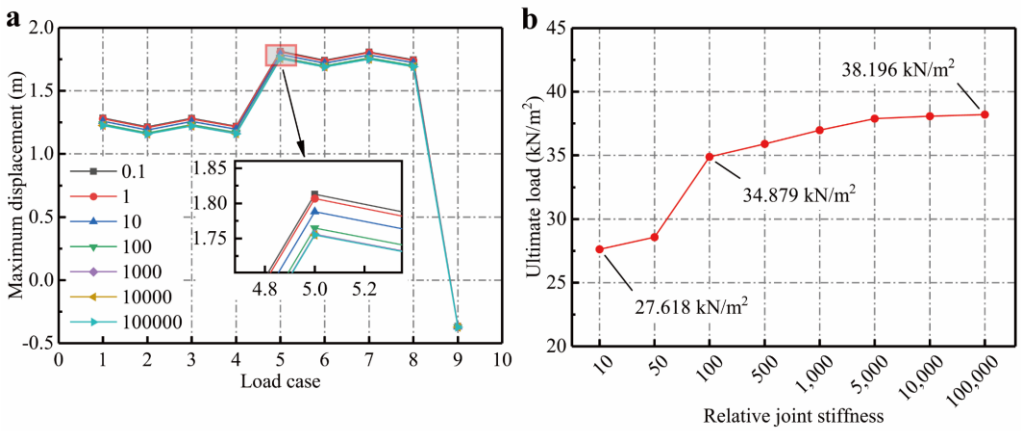


Figure 4: Static and stability calculation results for structures with different joint stiffness, a) maximum displacement, b) ultimate load.

## 4. A comparison of structures with two materials

In this section, the Three-dimensional structures with spans of 800m, 1000m, and 1200m, constructed using steel or aluminum alloy, were analyzed, and compared in terms of static and stability performance. Based on Zhang et al. [9], the following parameters were adopted. The rise-span ratio $H/L$ was assumed to be 1/4. The circumferential divisions $C_g$, and $C_t$ of the two structures, as well as the number of radial grids $R$, were all 6. The internode length to total length ratio $m/l$ was 1/11, the height to total length ratio $h/l$ was 1/11 and the width to total length ratio $b/l$ the 3D trussed beams was 1.0.

### 4.1. Force distribution of structures with spans of 800m

The force distribution of a mega-latticed structure is more complicated than that of a single-layer latticed shell. In mega-latticed structures, the top and bottom chord members are the main bearing members. Before comparing the static properties and stability, the optimization results for chord member sections of an 800m Three-dimensional grid-type steel structure were set as an example to illustrate the force distribution, as shown in Figure 5. The red and blue circles represent sections of the top and bottom chord members of the 3D trussed beams respectively, and the size of these circles indicate the relative size of the section diameters. As for the radial 3D trussed beams, considering the changes from inner rings to outer rings, the diameters of the top chord members gradually decrease while the diameters of bottom chord members increase greatly. For the circumferential 3D trussed beams, the diameters of top and bottom chord members were close to those of the radial 3D trussed beams at the inner rings. At the outer rings, the diameters of top chord members decrease sharply while those of bottom chord members decrease slightly.

One possible explanation is as follows: As the radial and circumferential 3D trussed beams play different roles in the structures, they are discussed separately and the radial ones are first discussed. The mega-

latticed structures, mainly bear membrane forces under uniform vertical pressure, i.e. the 3D trussed beams are mainly compressed. Besides, there are also bending forces in the structures. It can be inferred from the displacement of the structures, as illustrated in Figure 5, that there are out-of-plane and inward bending forces on the inner rings, which leads to additional pressure on the top chord members and tension on the bottom chord members. In contrast, there are out-of-plane and outward bending forces at the outer rings, which leads to additional tension and pressure at the top and bottom chord members, respectively. These additional forces combine with the main membrane pressure and result in the difference between top and bottom chord members from the inner rings to the outer rings. In addition, loads on the inner rings all transfer to the supports of the outmost ring through the radial 3D trussed beams, which also leads to an increase of the chord member sections at the outer rings. For the circumferential 3D trussed beams, on the one hand, the membrane effect weakens from the inner rings to the outer rings. On the other hand, there are still out-of-plane and inward-bending forces on the inner rings. But at the outer rings, there is nearly no bending force, and these circumferential 3D trussed beams constrain the outward displacement tendency of the radial ones, which leads to additional tension at both top and bottom chord members of the circumferential 3D trussed beams and overlay on the original pressure. Therefore, the above two aspects result in the decrease of the chord member sections of the circumferential 3D trussed beams from the inner rings to the outer rings.

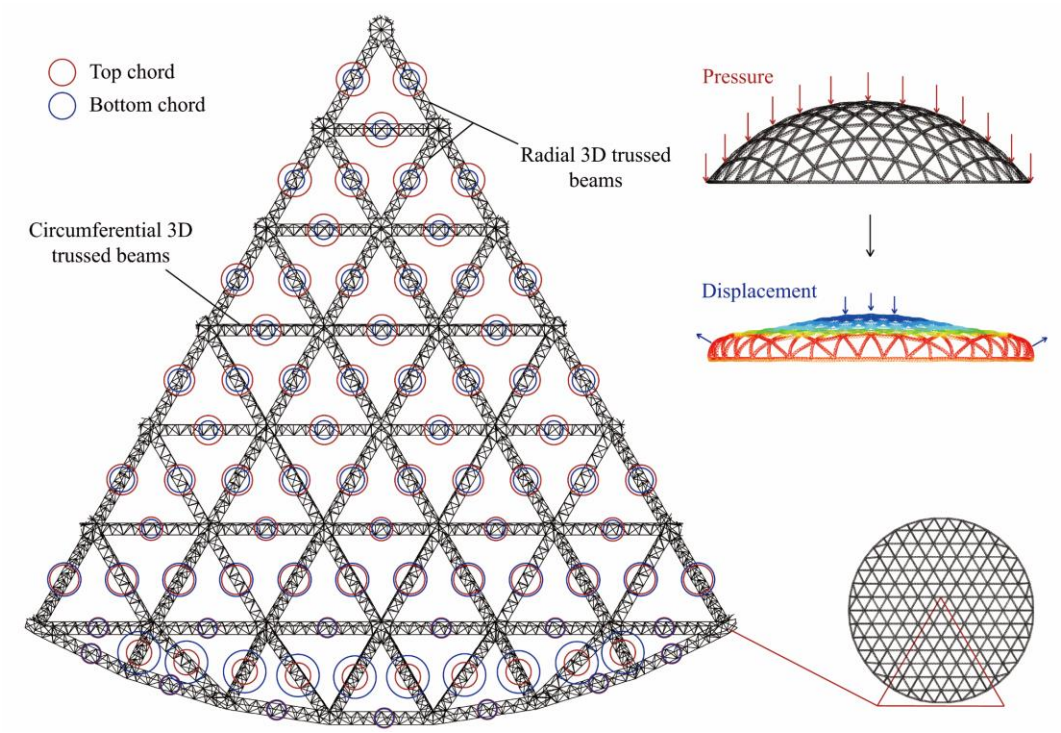


Figure 5: Chord member sections of the 800m span Three-dimensional grid-type steel structure after optimization.

It can be seen that the bending forces play an important role in the mechanical performance of the mega-latticed structures, which leads to obvious differences in the distribution of chord member sections from the inner rings to the outer rings. As aluminum alloy has qualitatively similar material properties to steel, the aluminum alloy structures have similar force distribution according to the optimization results. Because of the limitation of the length of the paper, no more illustrations are given here.

### 4.2. Static analysis of 800m span structures

The static calculation results for the 800m span Three-dimensional grid-type structures are shown in Table 3. For the steel structure, the least favorable load case was case 7 (as shown in Figure 6(a)), which consisted of uniform dead loads, half-span uniform live loads, and a decreased temperature. The maximum displacement was 0.861 m, which was 1/929 of the span. The sensitive coefficient of

temperature $f_T$ was 24.4%. The maximum upward displacement under case 9 was 0.095 m, as shown in Figure 7(a). For the aluminum alloy structure, the least favorable load case was case 8 (as shown in Figure 6(b)), which also consisted of uniform dead loads, half-span uniform live loads, and a decreased temperature, but had different partial and combination coefficients to case 7. The maximum displacement was 1.591 m, which was 1/503 of the span. The sensitive coefficient of temperature $f_T$ was 29.3%. The maximum upward displacement in case 9 was 0.757 m, as shown in Figure 7(b).

Table 3: Static calculation results for the 800m span three-dimensional grid-type structures.

| Material | Case number | Case 1 | Case 2 | Case 3 | Case 4 | Case 5 | Case 6 | Case 7 | Case 8 | Case 9 |
|---|---|---|---|---|---|---|---|---|---|---|
| Steel | Maximum displacement (m) | 0.683 | 0.636 | 0.692 | 0.651 | 0.853 | 0.805 | 0.861 | 0.819 | -0.095 |
| | Stress peak (MPa) | 287 | 269 | 292 | 292 | 277 | 261 | 292 | 283 | 252 |
| Aluminum alloy | Maximum displacement (m) | 1.046 | 1.048 | 1.078 | 1.098 | 1.370 | 1.372 | 1.400 | 1.420 | -0.757 |
| | Stress peak (MPa) | 149 | 150 | 169 | 185 | 154 | 155 | 155 | 171 | 182 |

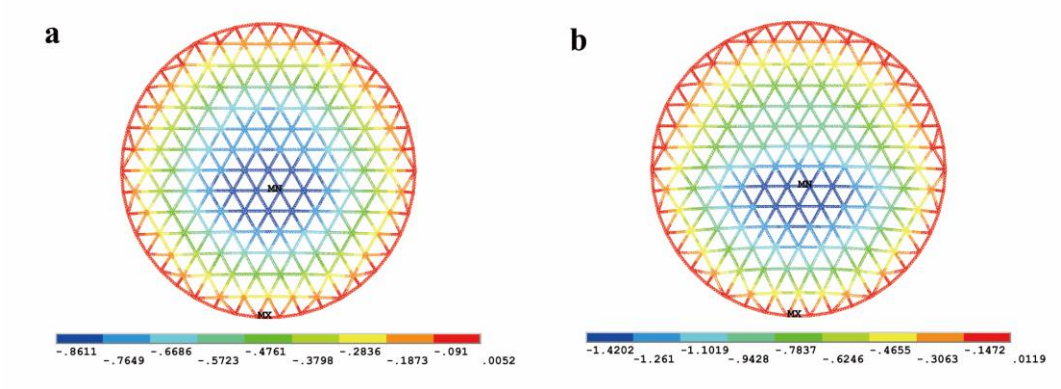


Figure 6: Distribution of displacements of the structures under the least favorable cases, a) steel (case 7), b) aluminum alloy (case 8).

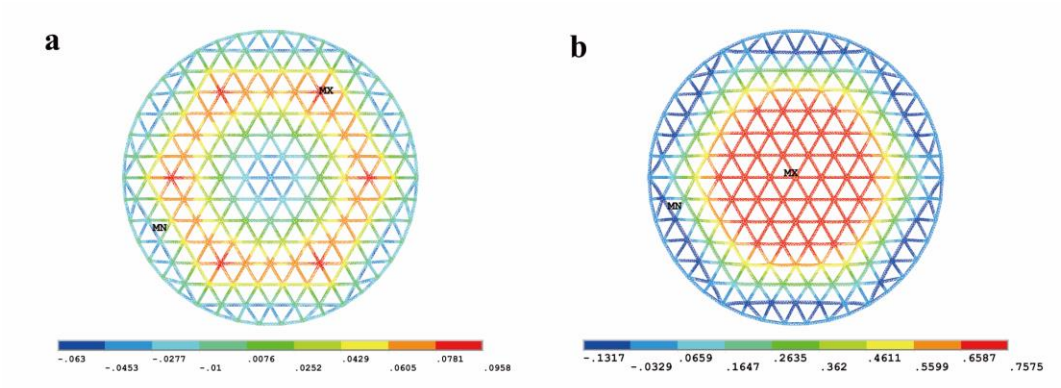


Figure 7: Distribution of displacements of the structures under case 9, a) steel, b) aluminum alloy.

Comparing the least favorable load cases, the aluminum alloy structures have lower structural stiffness than the steel structures, mainly because of the lower elastic modulus $E$ (mentioned in Section 2.1). However, the maximum displacements of the aluminum alloy structures completely satisfy the specification requirements. Although aluminum alloy has a higher thermal expansion coefficient $\alpha$ than that of steel, the aluminum alloy structures are nearly as sensitive as the steel structures to the change of temperature. Under load case 9, the maximum upward displacements of the aluminum alloy structures

are much bigger than those of the steel structures, which means that the aluminum alloy structures are more sensitive to wind. This is because of their lower structural weight and elastic modulus.

### 4.3. Stability analysis of structures with spans of 800m

Figure 8 shows the complete load-displacement curves and the ultimate loads for the 800m span Three-dimensional grid-type structures. For the steel structure, the ultimate load with no imperfections was 29.224kN/m$^2$. The ultimate loads decreased to 22.268kN/m$^2$ for elastic stability and 7.345kN/m$^2$ for elastoplastic stability with *L*/300 node imperfections. For the aluminum alloy structure, the ultimate load with no imperfections was 8.074kN/m$^2$. The ultimate loads decreased to 6.397kN/m$^2$ for elastic stability and 3.114kN/m$^2$ for elastoplastic stability with *L*/300 node imperfections. The deformations of these two structures under the ultimate loads of *L*/300 elastoplastic stability are illustrated in Figure 9, which shows both out-of-plane buckling forms. Similarly, it can be seen that the Three-dimensional grid type aluminum alloy structure has a lower bearing capacity and is less sensitive to node imperfections and elastoplastic stability than the steel ones. It should be noticed that the Three-dimensional grid-type structures are much less sensitive to node imperfections and elastoplastic stability, which leads to the higher bearing capacities of the former structures. A possible explanation for this difference in sensitivity is their different buckling forms.

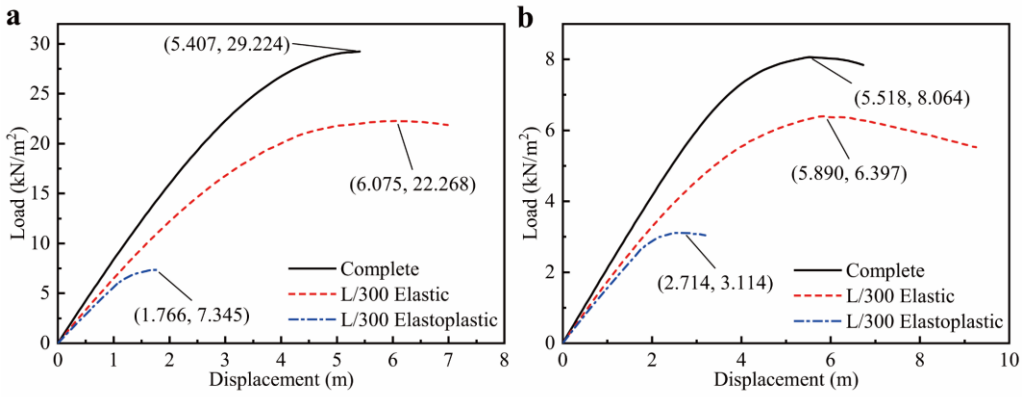


Figure 8: Load-displacement curves for the 800m span structures, a) steel, b) aluminum alloy.

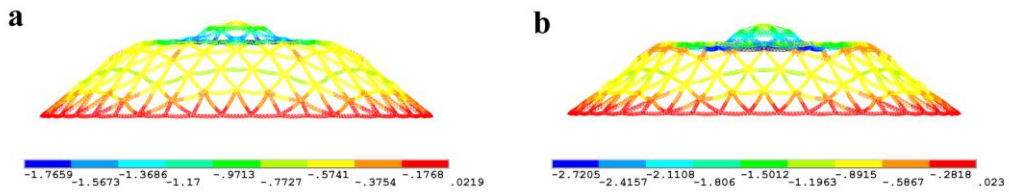


Figure 9: Deformation of the structures under ultimate loads, magnified by a factor of 30, a) steel, b) aluminum alloy.

### 4.4. Comprehensive analysis of structures with spans of 800m, 1000m and 1200m

Above all, for structures with spans of 800m, it can be concluded that the aluminum alloy structures have lower structural stiffness and bearing capacity than the steel ones, and they are more sensitive to wind but less sensitive to node imperfections and elastoplastic stability. As mentioned in Zhang et al. [8], the static and stability performance of the super-long span space structures may change dramatically with small increases in span. To investigate the differences in the static and stability performance of aluminum alloy and steel structures, spans of 1000m and 1200m were considered and the safety factors (ratio of ultimate load to standard load combination) for *L*/300 elastoplastic stability and the material consumption were calculated. The results are summarized in Table 4 for the Three-dimensional grid-type structures. For the Three-dimensional grid-type structures, the maximum displacements also increased gradually and the ultimate loads increased obviously with increasing span, whilst still meeting the specification requirements. But at the same time, the material consumption increased greatly. The

material consumption of the aluminum alloy structures was nearly 1/3, 1/5, and 1/7 of those of the steel structures.

Table 4: Static and stability calculation results for the structures with spans of 800m, 1000m, and 1200m.

| Material | Span (m) | Maximum displacement (m) | Stress peak (MPa) | Ultimate load (kN/m$^2$) | | | Safety factor | Material consumption (kg/m$^2$) |
|---|---|---|---|---|---|---|---|---|
| | | | | Complete | *L*/300 Elastic | *L*/300 Elastoplastic | | |
| Steel | 800 | 0.861 | 292 | 29.224 | 18.765 | 7.345 | 2.3 | 239.028 |
| | 1000 | 1.043 | 328 | 34.034 | 27.856 | 8.969 | 2.2 | 435.803 |
| | 1200 | 1.189 | 306 | 58.230 | 38.983 | 9.902 | 1.8 | 843.594 |
| Aluminum alloy | 800 | 1.420 | 185 | 8.074 | 6.397 | 3.087 | 2.6 | 72.192 |
| | 1000 | 1.833 | 184 | 8.801 | 6.445 | 3.248 | 2.5 | 96.127 |
| | 1200 | 2.146 | 179 | 9.775 | 7.288 | 3.413 | 2.4 | 129.896 |

Based on the above results, it can be concluded that the bearing capacity improves with increasing span. However, along with the improvements of bearing capacity, the material consumption increases greatly. The situation is different for aluminum alloy and steel structures, which shows that aluminum alloy structures are more economical at larger spans. Taking the 1200m span Three-dimensional grid type structures as an example, the material consumption for the steel structure is 843.594 kg/m$^2$, whilst that for the aluminum alloy structure is 129.896 kg/m$^2$. It should be mentioned that the ultimate loads and the material consumption of the steel structures seem higher than those of Zhang et al. [9] for the same span. This is mainly because of the different structural geometric parameters and loads. To sum up, the aluminum alloy structures have better economic indices than the steel structures when their spans are larger than 1000m. Thus, aluminum alloy can be used as a reasonable material for super-long span mega-latticed structures at spans of 1000m and 1200m.

## 5. Conclusions

In this paper, Three-dimensional grid-type aluminum alloy mega-latticed structures were generated using ANSYS. The joint stiffness of the structures was discussed and a proper simulation method for the joints in the FE model was proposed. A comparison of the super-long span Three-dimensional grid type mega-latticed structures using aluminum alloy and steel has been presented, based on their mechanical performance and economic indices. Suitable forms and spans of super-long span aluminum alloy mega-latticed structures have been investigated. It is shown that aluminum alloy is a suitable material for super-long span mega-latticed structures and reasonable structural parameters are proposed. The main conclusions from this work are:

(1) The joint stiffness and size of a joint have a relatively smaller effect on the mega-latticed structures than on single-layer latticed shells. For the mega-latticed structure, to save computing time, the joints are appropriate to be considered as rigid connections

(2) At spans from 800m to 1200m, the aluminum alloy structures have lower structural stiffness and bearing capacity than the steel structures; they are more sensitive to wind but less sensitive to node imperfections and elastoplastic stability.

(3) The material consumptions of the aluminum alloy structures were nearly 1/3-1/7 of those of the steel structures at spans from 800m to 1200m, indicating that the aluminum alloy structures have better economic indices at larger spans. Therefore, aluminum alloy can be used as a reasonable material for super-long span mega-latticed structures at spans of 1000m and 1200m.

## Acknowledgments

This work was financially supported by the National Natural Science Foundation of China (Grant no. 51508132, 51578186, and 51525802), which is gratefully acknowledged.

## References

[1] Z.S. Makowski, “Space Structures of Today and Tomorrow,” in Proceedings of third international conference on space structures, 1984, pp. 1-8.

[2] A.I. El-Sheik, "Development of a new space truss system," *J Constr Steel Res*, vol. 37, pp. 205-227, 1996.

[3] Y. He, X. Zhou, Y. Liu, et al. "Super-span reticulated mega-structure," *Journal of Architecture and Civil Engineering*, vol. 22, no. 3, pp. 25-29, 2005. (in Chinese).

[4] Y. He, and X. Zhou, "Static properties and stability of cylindrical ILTDBS reticulated mega-structure with double-layer grid substructures," *J Constr Steel Res*, vol. 63, pp. 1580-1589, 2007.

[5] X. Zhou, Y. He, and L. Xu, "Formation and stability of a cylindrical ILTDBS reticulated mega-structure braced with single-layer latticed membranous shell substructures," *Thin Wall Struct*, vol. 47, pp. 537-546, 2009.

[6] X. Zhou, Y. He, and L. Xu, "Stability of a cylindrical ILTDBS reticulated mega-structure with single-layer LICS substructures," *J Constr Steel Res*, vol. 65, pp. 159-168, 2009.

[7] Y. He, and X. Zhou, "Formation of the spherical reticulated mega-structure and its stabilities in construction," *Thin Wall Struct*, vol. 49, pp. 1151-1159, 2011.

[8] Q. Zhang, Y. Zhang, L. Yao, et al. "Finite element analysis of the static properties and stability of a 800m Kiewitt type mega-latticed structure," *J Constr Steel Res*, vol. 137, pp. 201-210, 2017.

[9] Q. Zhang, Y. An, Z. Zhao, et al. "Model selection for super-long span mega-latticed structures," *J Constr Steel Res*, vol. 154, pp. 1-13, 2019.

[10] Y. Tan, Y. Zhang, Q. Zhang, et al. "Static properties and stability of super-long span aluminum alloy mega-latticed structures," *Structures*, vol. 33, no. 3, pp. 3173-3187, 2021.

[11] Y. Tan, Y. Zhang, Q. Zhang, et al. "A conceptual design approach for mega-latticed structures based on combinatorial equilibrium modelling," *Eng. Struct*, vol. 306, pp. 117833, 2024.

[12] F.M. Mazzolani, "3D aluminium structures," *Thin Wall Struct*, vol. 61, pp. 258-266, 2013.

[13] Z. Xiong, X. Guo, Y. Luo, et al. "Elasto-plastic stability of single-layer reticulated shells with aluminium alloy gusset joints," *Thin Wall Struct*, vol. 115, pp. 163-175, 2017.

[14] Z. Xiong, X. Guo, Y. Luo, et al. "Experimental and numerical studies on single-layer reticulated shells with aluminium alloy gusset joints," *Thin Wall Struct*, vol. 118, pp. 124-136, 2017.

[15] China Architecture & Building Press, *GB 50009-2012: Load code for the design of building structures*, Beijing, 2012. (in Chinese).

[16] F. Fan, Z. Cao, and S. Shen, "Elasto-plastic stability of single-layer reticulated shells," *Thin Wall Struct*, vol. 48, pp. 827-836, 2010.

[17] China Architecture & Building Press, *JGJ 7-2010: Technical specification for space frame structures*, Beijing, 2010. (in Chinese).

[18] M.A. Crisfield, "An arc-length method including," *Int J Numer Meth Eng*, vol. 19, pp. 1269-1289, 1983.

[19] E. Riks, "An incremental approach to the solution of snapping and buckling problems," *Int J Solids Struct*, vol. 15, pp. 529-551, 1979.

[20] F. Fan, J. Yan, and Z. Cao, "Elasto-plastic stability of single-layer reticulated domes with initial curvature of members," *Thin Wall Struct*, vol. 60, pp. 239-246, 2012.

[21] SAS IP, Inc., *ANSYS, Inc. Theory Manual. 001369.* (12th ed.), 2009.

[22] H. Ma, F. Fan, J. Zhong, et al. "Stability analysis of single-layer elliptical paraboloid latticed shells with semi-rigid joints," *Thin Wall Struct*, vol. 72, pp. 128-138, 2013.

*Proceedings of the IASS 2024 Symposium*
*Redefining the Art of Structural Design*
August 26-30, 2024, Zurich Switzerland
Philippe Block, Giulia Boller, Catherine De Wolf,
Jacqueline Pauli, Walter Kaufmann (eds.)

# Copyright Declaration

Before publication of your paper in the Proceedings of the IASS Annual Symposium 2024, the Editors and the IASS Secretariat must receive a signed Copyright Declaration. The completed and signed declaration may be uploaded to the EasyChair submission platform or sent as an e-mail attachment to the symposium secretariat (papers@iass2024.org). A scan into a .pdf file of the signed declaration is acceptable in lieu of the signed original. In the case of a contribution by multiple authors, either the corresponding author or an author who has the authority to represent all the other authors should provide his or her address, phone and E-mail and sign the declaration.

Paper Title: Super-long span aluminum alloy mega-latticed structures

Author(s): Qingwen ZHANG*, Yilinke TAN[a], Guolong ZHANG, Yu ZHANG, Feng FAN

Affiliation(s): * School of Civil Engineering, Harbin Institute of Technology
[a] School of Architecture and Civil Engineering, Xihua University

Address: * Huanghe Road 73, Harbin 150090, China
[a] Tuqiaojin Road 999, Chengdu 610039, China

Phone: +86 15045811536

E-mail: zhangqw@hit.edu.cn

I hereby license the International Association for Shell and Spatial Structures to publish this work and to use it for all current and future print and electronic issues of the Proceedings of the IASS Annual Symposia. I understand this licence does not restrict any of the authors' future use or reproduction of the contents of this work. I also understand that the first-page footer of the manuscript is to bear the appropriately completed notation:

> *Copyright © 2024 by <name(s) of all of the author(s)>*
> *Published by the International Association for Shell and Spatial Structures (IASS) with permission*

If the contribution contains materials bearing a copyright by others, I further affirm that (1) the authors have secured and retained formal permission to reproduce such materials, and (2) any and all such materials are properly acknowledged by reference citations and/or with credits in the captions of photos/figures/tables.

Printed name: Qingwen Zhang Signature: Qingwen Zhang

Location: Harbin, China Date: 02/06/2024